Assessment of Carbon-Titanium Multilayer Coatings on Aluminum as Bipolar Plates in PEM Fuel Cells

Dabiri Havigh, Meisam; Hubin, Annick; Terryn, Herman

Published in:
Journal of the Electrochemical Society

DOI:
10.1149/1945-7111/ac0652

Publication date:
2021

Assessment of carbon-titanium multilayer coatings on aluminum as bipolar plates in PEM Fuel Cells

Meisam Dabiri Havigh[1], Annick Hubin[1], Herman Terryn[1,z]

[1]Department of Materials and Chemistry, Research Group Electrochemical and Surface Engineering (SURF), Vrije Universiteit Brussel, Pleinlaan 2, 1050 Brussels, Belgium

[z] Corresponding author: Herman Terryn (herman.terryn@vub.be)

Abstract

Aluminum is an appropriate candidate for bipolar plates in proton exchange membrane (PEM) fuel cells because it reduces the final cost and weight of the fuel cell stack in comparison to stainless steel, titanium and graphite. However, a conductive coating layer is essential to protect it against corrosion. In this study, the electrochemical behavior of aluminum coated with titanium and amorphous carbon layers by physical vapor deposition is evaluated. The main goal is to investigate the corrosion protection performance and the possible failure reasons of the coating in sulfuric acid solutions (with different pH values) in the presence of 3 ppm sodium fluoride and elevated temperature (80 ˚C) to mimic the working conditions of PEM fuel cells. To reach our aim, electrochemical tests are combined with surface analysis techniques. It is revealed that at low pH values (pH= 2 and 3), the coating fails due to the acidity of the electrolyte solutions. However, in the electrolyte with pH= 4, present fluoride ions interfere and consequently lead to localized failures. It is noticed that the presence of defects in the coating is a key parameter in the application of coated aluminum as bipolar plates in PEM fuel cells.

Keywords: Fuel cell, Bipolar plate, Coated aluminum, Corrosion, Fluoride ion

Introduction

Nowadays, due to the huge consumption rate of energy, we are facing an energy crisis in all aspects of our lives, among others in the transportation sector. One of the promising solutions is hydrogen-based economy in which fuel cells have attracted a great deal of attention [1], [2].

Fuel cells are electrochemical devices that convert the chemical energy of reactants (a fuel and an oxidant) into electricity and water as the only byproduct. Amongst different types of fuel cells, Proton Exchange Membrane (PEM) fuel cells are considered an appropriate candidate for the automotive industry because of their high energy density, high efficiency, zero emission, fast start-up (due to the solid immobile electrolyte), continuous operating and low operation temperature (50 to 100 ˚C) [2-8].

As such, PEM fuel cells are a clean and renewable source of energy in the automotive industry. However, one of the main challenges in the wide range of applications of the fuel cell technology is its high cost that should be reduced. The bipolar plates constitute about 80% of the weight and more than 40% of the total stack cost of PEM fuel cells [3-5, 9, 10]. Hence, finding a cost-effective material for the bipolar plates can pave the path for the commercialization of PEM fuel cells and enable them to compete with other energy sources (like fossil fuels) in the automotive industry [2]. Bipolar plates are multi-functional components that conduct the current from cell to cell, facilitate thermal and water management and distribute reactant gases in fuel cells [5, 11, 12]. Bipolar plate materials should also be electrically conductive, gas impermeable and low cost to meet PEM fuel cells requirements.

Traditionally, graphite was the main choice for the bipolar plate fabrication due to its conductivity and high corrosion resistance in the working environment of fuel cells. However, gas permeability, low mechanical strength and the expensive machinery cost hindered its application in the fuel cell technology [8, 13-15]. Metallic materials like stainless steel and titanium have been proposed as bipolar plate materials because of their gas impermeability, high mechanical strength, high thermal and electrical conductivity [3, 4, 13]. Nevertheless, the high weight of stainless steel and expensive and time consuming machinery of titanium (because of its inherent hardness) as well as the corrosion of these metals necessitate finding another alternative material for the bipolar plates [16]. A typical PEM fuel cell in the automotive application contains 740 bipolar plates [16]. Therefore, light weight and cost-effective bipolar plate materials can lead to huge cost and weight reduction. Moreover, the corrosion of metallic bipolar plates can have some catastrophic consequences in the

fuel cell stack. First of all, the production of corrosion products in the form of oxides and hydroxides, which are non-conductive, may precipitate on the surface of bipolar plates and reduce the final output power of the fuel cell. Secondly, the metallic ions released as a result of metal oxidation can poison the membrane and the catalyst layer [17].

Aluminum can be an appropriate candidate for the bipolar plate material due to its gas impermeability and high mechanical strength with respect to graphite as well as formability, low machinery cost and light weight in comparison with titanium and stainless steel [3, 13, 18]. The main bottleneck of aluminum is corrosion in the working conditions of PEM fuel cells because the presence of an acidic environment (pH ≅ 3) along with fluoride ions (F^-) (washed away from membranes that act as an electrolyte in PEM fuel cells [19]) and elevated operation temperature (50 to 100 ℃) increase the corrosion rate of aluminum. Depositing a protective coating layer on the aluminum substrate has been recommended as a solution [16, 18, 20, 21].

Mawdsley and coworkers [16] have developed composite coatings of graphite, titanium carbide (TiC) and ethylenetetrafluoroethylene (ETFE) for the aluminum substrate for bipolar plates applications by the wet spraying method. They have reported that the anodic corrosion resistance requirements for coated aluminum were not satisfied in the working conditions of fuel cells due to the presence of porosity and pinholes in the microstructure of the coating deposited by the wet spraying process.

Joseph et al. [20] evaluated the corrosion properties of polyaniline and polypyrrole coated aluminum as bipolar plate materials in 0.1 M sulfuric acid solution (pH ≅ 3). In this research, the role of fluoride ions in the corrosion protection performance of the coating layer is not investigated and they have concluded that applied polymeric coatings have not improved the corrosion protection properties and the contact resistance.

Hung et al. [2] evaluated the lifetime of coated aluminum as bipolar plates in PEM fuel cells operating at 70 ℃. However, the role of fluoride ions on the corrosion of coated aluminum as bipolar plates and the dependency of fluoride ions activity on the pH values of acidic solutions in the fuel cell stack is not investigated.

Therefore, the present study focused on the evaluation of the corrosion protection performance and the possible failure of a carbon-titanium multilayer coating on the aluminum substrate in the working conditions of PEM fuel cells as a function of pH and the fluoride content of the electrolyte solution.

In this research, coated aluminum contains two layers of coating due to the fact that multilayer coatings have improved the corrosion resistance of coated bipolar plates in comparison to the single layer coatings [22]. The first layer is titanium on top of the aluminum substrate because titanium not only shows higher corrosion resistance in sulfuric acid solutions containing fluoride ions with concentrations below 0.002 M [23] but also improves the conductivity of bipolar plates [24]. The second layer is amorphous carbon on top of titanium to avoid immediate oxidation of titanium and reduce interfacial contact resistance (ICR) [25]. The coating layers are deposited by the physical vapor deposition (PVD) technique as it has been employed widely to deposit various coating layers including gold [26], amorphous carbon and metal nitrides such as titanium and chromium nitrides (TiN, CrN) [22] for fuel cell applications. In addition, this technique offers numerous advantageous like coating uniformity, good adherence, high film densities and high deposition rate [27]. To the best of our knowledge, the PVD deposited carbon-titanium multilayer coating has not yet been studied for aluminum as bipolar plate materials.

The pH values of the electrolyte solutions are chosen 2, 3 and 4 because PEM fuel cells are operational at pH $\cong$ 3 which is around the stability domain of aluminum. Moreover, 3 ppm (7.15×10^{-5} M) NaF is added to electrolyte solutions to investigate its effect on the corrosion behavior of the coating layer. To investigate the corrosion protection performance of the coating layer and study possible degradation reasons of it, electrochemical measurements, Open-Circuit-Potential (OCP) and Linear-Sweep-Voltammetry (LSV), are combined with the surface analysis techniques, Scanning Electron Microscopy (SEM), SEM coupled with an Energy Dispersive X-ray Spectroscope (SEM-EDX) and X-ray Photoelectron Spectroscopy (XPS). These techniques are selected for the following reasons:

The OCP measurement is an important test to evaluate the corrosion protection performance of the coating layer because the variation of the potential of the sample under investigation can easily be recorded over time. The LSV technique is used to evaluate the performance of the coating layer at elevated potential values because during the operation of PEM fuel cells, as a result of working under conditions like idling, load changing, start-up/shut-down the potential in the anode and cathode varies [28]. SEM is applied to study the morphology of the coating layer. EDX elemental analysis is used to do elemental analysis and detect the presence of the coating.

XPS is chosen in the current research to record depth profiles for coated samples to investigate the presence of the coating layer and examine whether there is an oxide layer at the interfaces of carbon

and titanium (C/Ti) and titanium and aluminum (Ti/Al). All surface analyses (SEM, SEM-EDX, XPS) are carried out for coated samples before and after electrochemical measurements.

It is worth noting that this is a type of coating layer under development and in the current study as the first investigation, the goal is to examine whether there is a potential for further development of this coating layer or not. Therefore, a limited amount of coated aluminum was supplied to do some preliminary measurements and that is why reported measurements in this paper are the results of single measurements.

Materials and Methods

Material

The working electrodes are bare and coated aluminum alloy 1050. In the current research, the aluminum substrate (AA1050) is coated with two layers of coating comprising titanium and amorphous carbon by the magnetron sputtering which is a PVD process. The thickness of the coating layer and the percentage of the sp^2 and sp^3 hybridizations of carbon atoms in the amorphous carbon layer of the coating will be discussed below. Specimens are cut in square shapes with the size of 1.5 cm by 1.5 cm. The coated samples are supplied by a company.

Electrolyte solution

Electrolyte solutions are prepared by addition of concentrated sulfuric acid (H_2SO_4) (analytical grade, Merck) to Milli-Q water (resistivity 18 MΩ.cm) to obtain the desired pH values and the pH values of the solutions is measured by Metrolab pH meter at room temperature. To investigate the corrosion protection performance of the coating in the presence of fluoride ions, 3 mg per liter sodium fluoride (NaF) is added to the acidic solutions with desired pH values to obtain solutions containing 3 ppm NaF [29] to mimic working conditions of PEM fuel cells. The activity of fluoride ions in acidic solutions is measured through a fluoride Ion Selective Electrode (ISE) (from Xylem Analytics) in conjunction with an Ag/AgCl reference electrode at room temperature due to the limitation of the equipment to be used at higher temperatures. It should be noticed that the solubility of NaF in water is linearly dependent on temperature [30] and allows to our assumption that the difference in the activity of fluoride ions in solutions with different pH values at room temperature will remain constant in the same solutions at elevated temperatures.

Electrochemical measurements

All electrochemical measurements are conducted in a three-electrode cell setup using an Autolab PGSTAT12 Potentiostat/Galvanostat which is controlled by NOVA software. In the setup, a platinum (Pt) mesh is used as the counter electrode, Ag/AgCl saturated with KCl solution as the reference electrode and bare and coated aluminum specimens as the working electrodes.

The OCP measurements are recorded for 24 hours and the LSV measurements are carried out from 50 mV below OCP to 1300 mV vs Ag/AgCl with a scan rate of $1mVs^{-1}$. The stabilization period prior to the LSV measurements is 15 minutes. All measurements are done in deaerated H_2SO_4

solutions with pH= 2, 3, 4 (with and without the presence of 3 ppm NaF).

All electrolytes are deaerated for 15 minutes before the onset of the experiments and also during the experiments by purging nitrogen gas. The three-electrode cell set up contains two holes on top to let nitrogen gas out of the cell. The temperature of the electrolyte solutions is maintained at 80 ± 1 ℃ during experiments.

SEM-EDX analysis

In order to characterize the surface of the coating before and after electrochemical measurements, the samples are analyzed by a JEOL JSM-IT300 Scanning Electron Microscope (SEM). It is coupled with an Oxford Instruments SDD X-MaxN 80 mm^2 Energy Dispersive X-ray spectroscope (EDX) to perform elemental analysis. The accelerating voltage for the SEM imaging and the EDX elemental analysis is 15 kV and 5 kV, respectively.

XPS analysis

The samples are analyzed by an X-ray Photoelectron Spectroscope, Versaprobe II and all spectra are detected by using an Al Kα X-ray operating at 25 W, a pass energy of 11.75 eV for high resolution and 187.5 eV for survey with an X-ray spot size of 100 µm.

XPS depth profiles are performed by argon ions (Ar^+) sputtering at 3 kV with steps of 0.5 min. The calibrated sputter rate is 25 nm min^{-1} for SiO_2. The pressure of the analysis chamber is maintained at 10^{-8} Torr during the analysis and depth profiles data is treated with PHI Multipak software. CasaXPS software is used to fit the high resolution spectra of C 1s with a Shirley type background and a Gaussian-Lorentzian peak shape. The energy scale of the XPS spectra is calibrated respect to the binding energy of the C 1s peak at 284.4 eV.

Results

The measurement of fluoride ions concentration

In this study, in order to investigate the influence of fluoride ions (F^-) on the corrosion of coated aluminum as bipolar plates in the PEM fuel cell stack, dependency of the activity of F^- on the pH values of acidic solutions is evaluated. Theoretically, by addition of 3 mg NaF per liter of an aqueous solution, in the case of complete dissociation of NaF, the concentration of fluoride ions should be 7.1×10^{-5} M. However, due to incomplete dissociation and the association of F^- with hydrogen ions (H^+) in acidic solutions according to Eq.1, the activity of F^- can deviate from theoretical calculations. Therefore, the evaluation of the activity of F^- in acidic solutions is important to elaborate its effect on the corrosion of bipolar plates. Thermodynamically, Eq.1 indicates that at pH values above 3.17, the reaction will proceed toward the dissociation of HF and F^- will be the predominant species in the solution while for pH values lower than 3.17, mainly HF will be present in the solution [31].

$$HF \leftrightarrow H^+ + F^- \qquad pKa = -\log Ka = 3.17 \ [31] \qquad (1)$$

where Ka is acid dissociation constant.

To prove the dependency of the activity of F^- to the pH value of acidic solutions experimentally, the activity of F^- is measured by the fluoride ISE. Measurements show that the activity of F^- is 5.2×10^{-6} M, 3.3×10^{-5} M and 4.6×10^{-5} M in solutions with pH = 2, 3 and 4, respectively. So practical measurements are in line with thermodynamics and the activity of F^- in the solution with pH=4 is higher than that in solutions with pH=2 and 3.

Electrochemical measurements

Open-Circuit-Potential (OCP) measurements

According to figure 1, OCP values for coated aluminum are more positive than that for bare aluminum (at all pH values). However, by increasing the immersion time, OCP values for coated samples immersed in electrolytes with pH=2 and 3, are getting more negative and show a tendency to move toward the OCP values of bare aluminum. As shown in figures 1a and 1b, after around

15 hours and 17 hours immersion in electrolytes with pH=2 and 3 respectively, OCP values of bare and coated aluminum are almost the same. Moreover, the initial rapid drop of OCP values of coated and bare samples in these solutions can be attributed to the dissolution of the aluminum oxide formed on the defects of the coating and on the surface of bare samples because the dissolution rate of the aluminum oxide is highly dependent on pH values of the solution and shows a sharp increase in low pH values [32].

According to figure 1c, in the electrolyte with pH=4, which based on the Pourbaix diagram is the thermodynamic stability region of the aluminum oxide layer, coated samples show stable and more noble OCP values than bare samples during 24 hours immersion. Also, the OCP values do not indicate an initial rapid drop meaning that the dissolution rate of the oxide layer is much less in comparison with that in pH values below 4. However, in the presence of fluoride ions, the dissolution of the oxide layer will be affected by both pH and the F^- concentration of the solution. Therefore, for the coated sample immersed in the electrolyte with pH=4 without the presence of fluoride ions, the passivation is already started but in the solution containing fluoride ions, there is a competition between the oxide film dissolution and re-passivation. That is why there is not a potential dip (dropping to a minimum and then rising to a plateau) for the coated sample in the solution with pH=4 in the absence of fluoride ions. Also, this explains that for bare aluminum in the solution with pH=4 (containing F^-) OCP results show a kind of similar evolution like typical conversion systems where fluoride ions are added to de-passivate the metal and form new film [33].

In addition, there is a difference between the OCP behavior of the coated and bare samples in the solution with pH=4 without the presence of fluoride ions that can be due to the relative surface area of the oxide layer exposed to the electrolyte. For the bare sample, the whole surface is exposed to the electrolyte while for the coated sample only the defects are exposed. This means that the anodic/cathodic surface area is different between two systems.

Therefore, OCP results indicate that the coating layer can resist initially in electrolyte solutions with pH=2 and 3 but after a while it fails. However, in the case of the electrolyte with pH=4, the coating layer shows a corrosion protection performance during 24 hours. In addition, in the electrolyte with pH=4, the presence of 3 ppm NaF has made the OCP values of coated and bare aluminum more negative in comparison with same samples immersed in the electrolyte with the same pH value without the presence of NaF. While in electrolyte solutions with pH=2 and 3 the

presence or absence of NaF has not affected OCP values. This may be due to the higher activity of F^- in the electrolyte with pH=4.

Potentiodynamic polarization measurements

Anodic polarization curves are recorded for coated and bare samples in electrolyte solutions with pH=2, 3 and 4 (with and without 3 ppm NaF) due to the competition in between the oxide film dissolution and re-passivation in acidic solutions containing F^- ions. Based on the LSV measurement results (figure 2), it is shown that the corrosion potential (E_{corr}) of coated aluminum is more noble than E_{corr} of bare aluminum. It is also noticed that the measured current density for coated aluminum is less than that for bare aluminum in low applied potentials. All these results indicate the corrosion protection performance of the coating layer. Furthermore, as shown in figure 2c, in the electrolyte with pH=4, the presence of 3 ppm NaF has made the E_{corr} of the coated sample more negative. However, for pH values of 2 and 3, the presence of NaF has not affected E_{corr} of coated samples.

Therefore, it can be concluded that the presence of NaF in the electrolyte solution with pH=4 has changed the electrochemical behavior of bare and coated aluminum, while it is not the case for samples immersed in other electrolyte solutions.

Surface analysis

Scanning Electron microscope (SEM) analysis

Figure 3 shows SEM images of the surface and cross-section of coated samples before (figure 3a and 3b) and after 24 hours OCP measurements in electrolyte solutions with pH= 2, 3 and 4 (all solutions contain 3 ppm NaF) at elevated temperature of the solutions (80 ℃). Based on figure 3b, the thickness of the coating layer (the combination of titanium and amorphous carbon layers) before exposure to the electrolyte solutions is approximately 500 nm, and the presence of defects is shown. For coated aluminum after the OCP measurement in the electrolyte solution with pH=2 (figure 3c), the coating is totally removed and the surface of the aluminum substrate is attacked by the acidic solution and the presence of holes is visible on the substrate. The removal of the coating is proved by the EDX elemental analysis in the next section. For the coated sample immersed in the electrolyte solution with pH=3 (figure 3d), the partial removal and the delamination of the coating layer is obvious. For the immersed sample in the electrolyte solution with pH=4 (figure 3e), the coating looks undamaged and that might be due to the low acidity of the solution.

SEM analysis is also performed for samples after LSV measurements in solutions with pH=2, 3 and 4 (all solutions containing 3 ppm NaF) and images are shown in figure 4.

Figure 4a shows the SEM image of the coated sample after the LSV measurement in the electrolyte with pH=2, which does not show an obvious damage in the coating that can be attributed to the lower F^- activity in the solution or the short experiment time in comparison to the OCP measurements. According to figure 4b and 4c, cracks are observed in the coating of the samples immersed in the electrolyte with pH=3 and 4. The black spot in figure 4b may be the local acidic attack of the substrate. The failure of the coating during the LSV measurement in electrolytes with pH=3 and 4 may happen at potentials above 500 mV vs Ag/AgCl because above that potential, the current density of coated and bare aluminum tends to get equal as shown in figures 2b and 2c.

EDX elemental analysis

EDX elemental analysis is performed for coated aluminum before and after 24 hours OCP measurements in electrolyte solutions with pH=2, 3 and 4 (all containing 3 ppm NaF) and temperature of 80 ℃. According to the results (table1), for the coated sample before exposure to electrolyte solutions, the presence of coating elements including carbon and titanium is shown. For the coated sample after the OCP measurement in the electrolyte with pH=2, titanium is totally removed and the atomic percentage of carbon has reduced significantly. Moreover, the atomic percentage of aluminum has increased in comparison to that for coated aluminum before exposure to the electrolyte. For the coated sample immersed in the electrolyte with pH=3, EDX elemental analysis is performed at two different places of the same sample (as shown in figure 3d). According to table1, in spectrum 1, the atomic percentage of carbon and titanium is 5 At% and zero respectively and the main element is aluminum with atomic percentage around 90 At%. However, for the same sample in spectrum 2 the presence of coating elements is obvious and the atomic percentage of aluminum is much less. Also, a small amount of sulfur is detected which can come from sulfuric acid solution used as the electrolyte.

Furthermore, the atomic percentage of elements for coated aluminum before and after the OCP measurement in the electrolyte with pH=4 is almost equal.

EDX elemental analysis proves the removal of the coating layer for the sample immersed in the electrolyte with pH=2. Moreover, the partial removal of the coating layer is also proved for the sample immersed in the electrolyte with pH=3. In addition, results indicate that the coating layer

looks undamaged after the OCP measurement in the electrolyte solution with pH=4. It should be noticed that fluoride could not be detected for samples after OCP measurements in electrolyte solutions containing fluoride ions and it can be due to the very small amount of added NaF.

EDX elemental analysis is also carried out for coated samples after LSV measurements (scanning starts for 50 mV below OCP till 1300 mV vs Ag/AgCl with scan rate of $1mVs^{-1}$) in electrolyte solutions with pH=3 and 4 in the cracks and failed parts of the coating (as shown in figure 4b and 4c). Based on the obtained results, summarized in table 2, the atomic percentage of all corresponding elements is almost the same for both samples. A very low percentage of fluoride is detected for the sample immersed in the electrolyte with pH=4 after the LSV measurement while it is not the case for other samples. Due to the low amount of added NaF (3 ppm) to solutions, very low percentage of detected fluoride is logical however experiments should be repeated at high concentrations of NaF.

There can be two possible explanations for the detection of fluoride ions in the case of sample immersed in the electrolyte with pH=4 after the LSV measurement. First, based on Eq.1 and experimental measurements with fluoride ISE, the maximum activity of F^- can be obtained in the electrolyte with pH=4 and the second reason is that by applying an anodic potential during the LSV measurement, formed aluminum ions can react with the fluoride ions in the solution. This can be a possible explanation why EDX elemental analysis cannot show the presence of fluoride ions on the surface of the coating after the OCP measurement in contrast to the LSV measurement.

XPS Analysis

XPS depth profiles are performed by argon ions (Ar^+) sputtering for coated samples before and after OCP measurements. Figure 5a shows the depth profiles of coated aluminum before exposure to the electrolyte. It is shown that carbon, titanium and aluminum appear respectively in the expected order as sputtering proceeds. It is important to notice that XPS depth profiles for coated aluminum before exposure to the electrolyte solution do not show the presence of an oxide layer at the interfaces of C/Ti and Ti/Al. Initially, the atomic concentration of oxygen is almost zero but after 15 minutes sputtering arises to around 10 % which can be due to the reoxidation of aluminum in the low pressure environment present in the XPS analysis chamber.

Murata et al. [34] have proved that the reoxidation of aluminum in low pressure environments (10^{-8} Torr) shows initially a slow rate and abruptly increases after 20 minutes which is in line with

the logarithmic growth rate of the aluminum oxide proposed by Mott [35].

Moreover, high resolution XPS spectra for O1s at different sputtering times (figure 5b), do not show any peak in binding energy around 530 eV which typically corresponds to the metal oxide binding energy [36].

XPS depth profiles of the coated sample before exposure to the electrolyte solution are used to estimate the thickness of coating layers. According to literature [37] the sputtering rate of TiO_2 is almost the half of that for SiO_2. Therefore, as an estimation, the thickness of the titanium layer can be (sputtering rate × sputtering time) approximately 300 nm. The thickness of the amorphous carbon layer can be 200 nm because as shown in SEM image (figure 3b), the total thickness of the coating layer is almost 500 nm. It should be emphasized that these values are rough estimations.

The C 1s peak decomposition, figure 5c, is performed after 3 minutes sputtering for the coated sample before exposure to the electrolyte solution to investigate the percentage of sp^2 and sp^3 hybridized carbon atoms in the amorphous carbon layer of the coating. The difference between sp^2 and sp^3 peak positions is kept constant (0.9 eV) in the peak decomposition process [38]. The results are available in table 3.

The number of carbon atoms in sp^2 and ps^3 hybridizations is proportional to the area under the corresponding peak divided by the sensitivity factor of the carbon atom [39]. As the sensitivity factor for XPS core-level spectra is only dependent on the atomic factors and not dependent on the chemical state of the atom [39], therefore, it should be constant for carbon atoms. Thus, the ratio of carbon atoms involved in sp^2 and sp^3 hybridizations is equal to the area of the sp^2 peak divided by the area of the sp^3 peak.

Based on table 3, by comparing the area of sp^2 and sp^3 peaks, it can be deduced that the percentage of sp^2 hybridized carbon atoms in the amorphous carbon layer of the coating is higher than that for sp^3 hybridized carbon atoms which can lead to the high electrical conductivity, hydrophobicity and chemical inertness of the coating layer [40].

XPS depth profiles are also recorded for coated samples after 24 hours OCP measurements in electrolyte solutions with pH=2, 3 and 4, all solutions containing 3 ppm NaF. For coated aluminum immersed in the electrolyte with pH=2, as shown in figure 5d, there is not any trace of titanium. Moreover, aluminum and oxygen appear from the first step of the sputtering. In the case of the coated sample after the OCP measurement in the electrolyte with pH=3, figure 5e, carbon and titanium are still present after 24 hours immersion but due to the lateral resolution of XPS, which

is in the order of micrometer, the partial removal of the coating , as shown in SEM and EDX elemental analysis, is not possible to show with this technique. In the case of coated aluminum immersed in the electrolyte with pH=4, XPS depth profiles results (figure 5f) show the presence of carbon and titanium on the aluminum substrate.

So the removal of the coating layer for the sample immersed in the electrolyte solution with pH=2 is proven by XPS as well. Also, depth profiles confirm the presence of the coating layer for the sample immersed in the electrolyte with pH=4 after the OCP measurements.

Discussion

According to the experimental results, it is shown that the coating layer has failed at pH values of 2 and 3 after OCP measurements and at pH values of 3 and 4 after LSV measurements. In this section, the possible failure reason of the coating is discussed. The failure of the coating can be attributed to the presence of some imperfections such as the porosity and the poor adhesion of the coating layer to the aluminum substrate. The presence of porosities in the coating acts as a pathway for the electrolyte which contains water molecules, ions including H^+, Na^+, F^-, OH^- and compounds like SO_4^{2-} to bring them to the interface of the coating and the substrate. When the electrolyte solution reaches the coating/substrate interface, based on the Pourbaix diagram, in acidic solutions with pH below 4, aluminum is unstable and its dissolution occurs at low oxidation potentials [41]. Therefore, aluminum starts to oxidize and produces aluminum ions and electrons. The produced electrons pass through the bulk of aluminum to reach local cathodic areas (mainly copper and iron in the case AA 1050). Consequently, the reduction of H^+ in the cathodic sites leads to the accumulation of hydrogen gas at the interface of the coating and the aluminum substrate along with the precipitation of corrosion products like aluminum oxide and hydroxide at the anodic sites [42]. This leads to the blistering and finally breaking down of the coating layer. A schematic overview of coated aluminum and the failure of the coating layer is shown in figure 6.

But for the coated sample after the LSV measurement in the electrolyte with pH=4 (containing 3 ppm NaF), which is the border of the passivity of aluminum [41], the presence of fluoride ions can interfere and lead to the localized failure of the coating as shown in figure 4c. After the failure of the coating, the aluminum substrate is exposed to an acidic electrolyte that contains fluoride ions. It is known that the presence of fluoride ions in electrolyte solutions increases the corrosion rate of aluminum [43], but its exact mechanism is not clear. Two possible mechanisms are proposed to

explain this phenomenon. Valand et al. [44] state that the substitutional incorporation of fluoride ions in the structure of the protecting oxide film weakens the protective properties of the oxide layer. Another view point relates the high corrosion rate to the adsorption and complex formation of fluoride ions with aluminum ions in the oxide layer which stimulates aluminum ions to transfer at the oxide/solution interface [43].

Concluding Remarks

In this study, the corrosion properties of coated aluminum as bipolar plate materials is investigated in the working conditions of PEM fuel cells. Based on the first assessment that is done so far in this work, experimental results proved that the electrochemical behavior of the coating layer depends on the pH and the activity of fluoride ions in the electrolyte solution.

Moreover, it was revealed that the coating layer shows an initial corrosion protection performance that, after a while (depending on pH and the fluoride ions activity) fails. In addition, the dependency of the activity of fluoride ions on the pH values of electrolyte solutions and its influence on the failure of the coating layer was investigated. The results indicated that, in low pH values of electrolyte solutions (pH=2 and 3), due to the low activity of fluoride ions, the failure of the coating layer happens mainly because of the acidity of electrolyte solutions. While in the electrolyte with pH=4, the presence of fluoride ions can interfere and lead to localized failures of the coating layer.

This preliminary study is performed with a limited amount of coated aluminum to evaluate the potential for further development of bipolar plates with the present coating layer. In order to have a broad view of the performance of this newly developed coating layer, its behavior should also be examined as a function of the fluoride content in electrolyte solutions. On the other hand, trying to provide coating layers with less defects or higher thicknesses can make aluminum more applicable in PEM fuel cells. In addition, as a future work, the presence of flaws and their dimensions should be investigated because the presence of defects in the coating layer plays a detrimental role in the corrosion protection performance.

We conclude that the preliminary results acquired so far can provide a new opportunity to develop cost and weight effective aluminum bipolar plates for the PEM fuel cell industry.

Figures and captions:

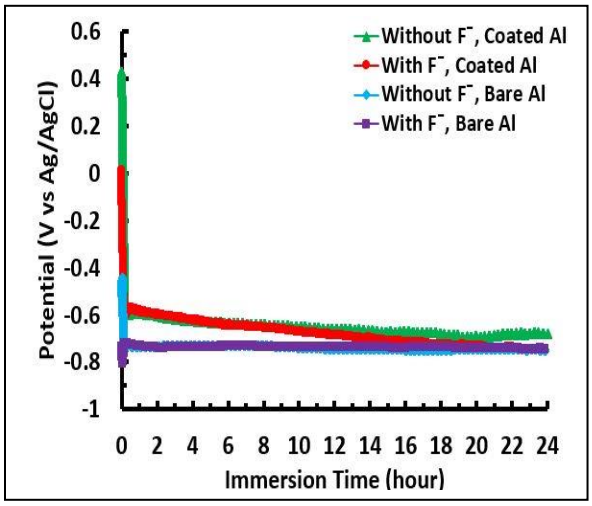

(a) The electrolyte solution with pH=2

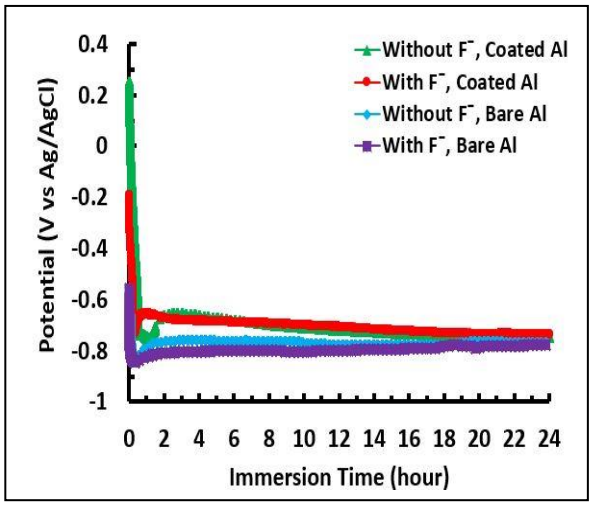

(b) The electrolyte solution with pH=3

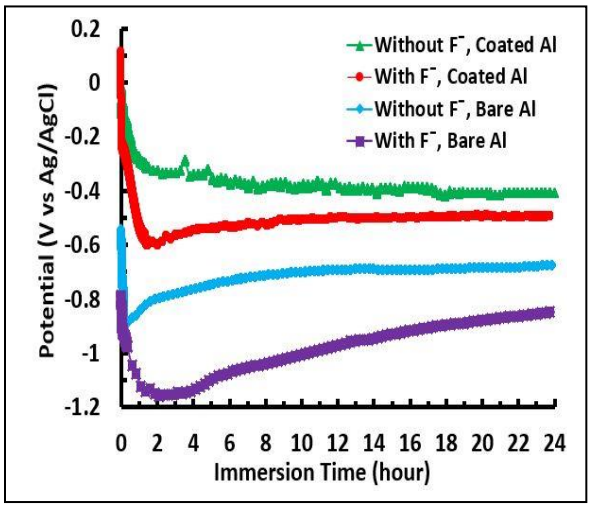

(c) The electrolyte solution with pH=4

Figure 1: OCP measurements for bare and coated aluminum in diluted sulfuric acid solutions with different pH values, a) pH=2, b) pH=3 and c) pH=4. Measurements are performed in solutions with and without the presence of 3 ppm NaF, measurement time=24 hours and solution temperature=80℃.

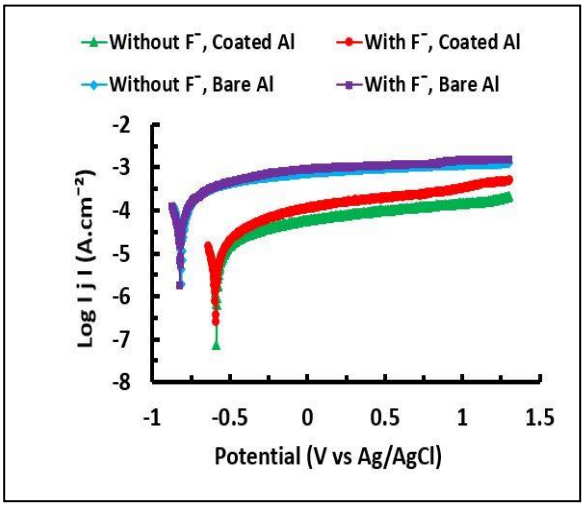

(a) The electrolyte solution with pH=2

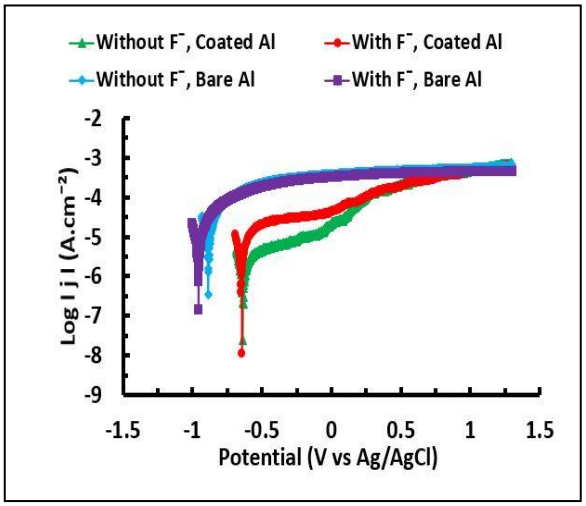

(b) The electrolyte solution with pH=3

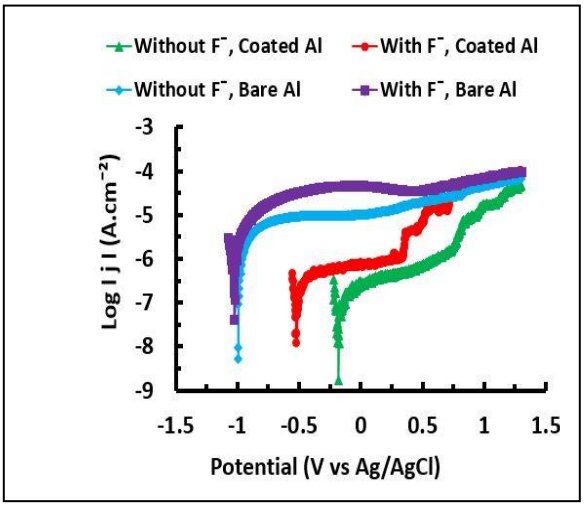

(c) The electrolyte solution with pH=4

Figure 2: LSV measurements for coated and bare aluminum, in electrolytes with a) pH=2,b) pH=3 and c) pH=4, solutions temperature=80 ℃, start potential=50 mV below OCP, end potential=1300 mV vs Ag/AgCl, scan rate=1 mVs^{-1}.

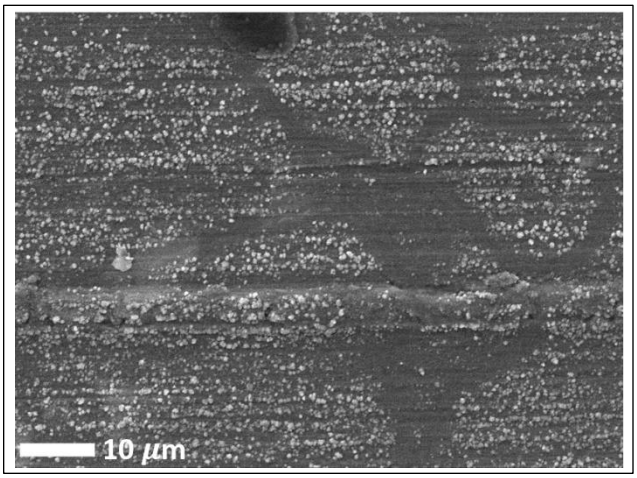

(a) Surface of coated Al before exposure to the electrolyte solution. Magnification ×1500

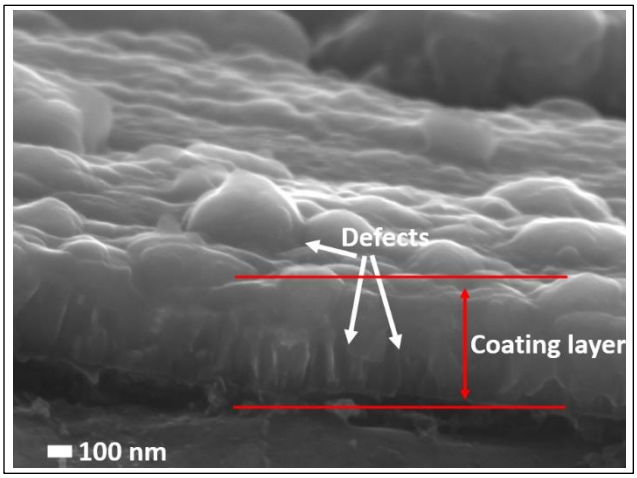

(b) Cross-section of coated Al before exposure to the electrolyte solution. Magnification ×50000

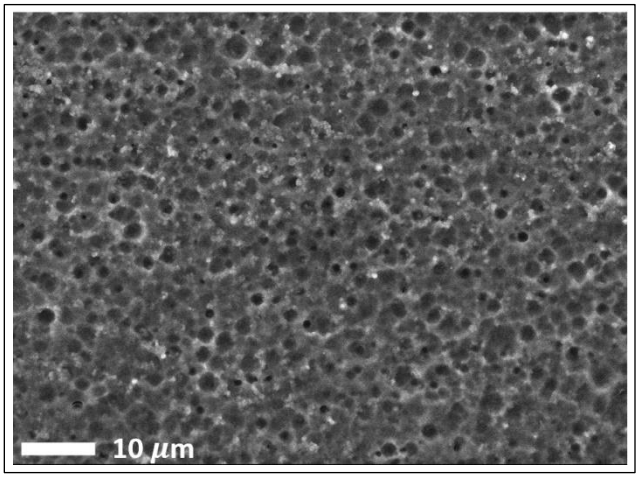

(c) Surface of coated Al immersed in the electrolyte solution with pH=2. Magnification ×1500

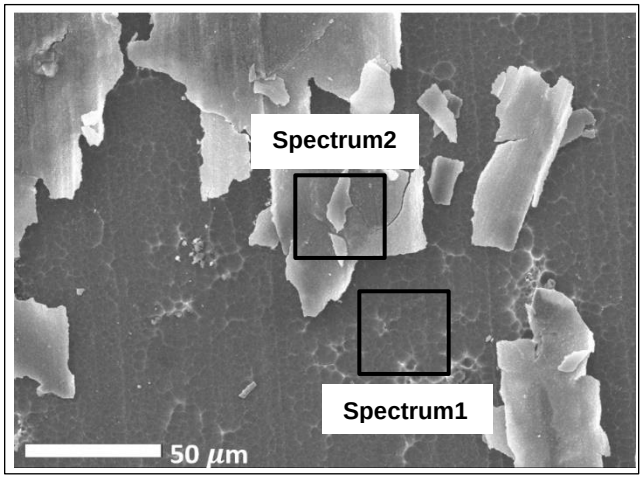

(d) Surface of coated Al immersed in the electrolyte solution with pH=3. Magnification ×500

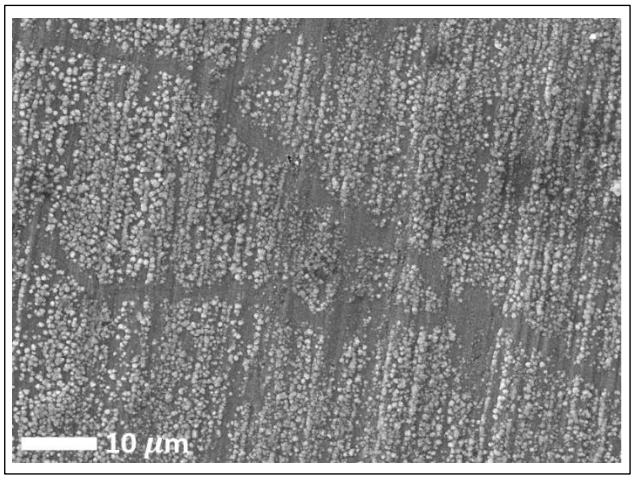

(e) Surface of coated Al immersed in the electrolyte solution with pH=4. Magnification ×1500

Figure 3: SEM images of the surface and the cross-section of coated aluminum before and after 24 hours OCP measurements, electrolyte solutions contain 3 ppm NaF, solution temperature=80 ℃ . Spectrum 1 and

2 show places where EDX elemental analysis was performed.

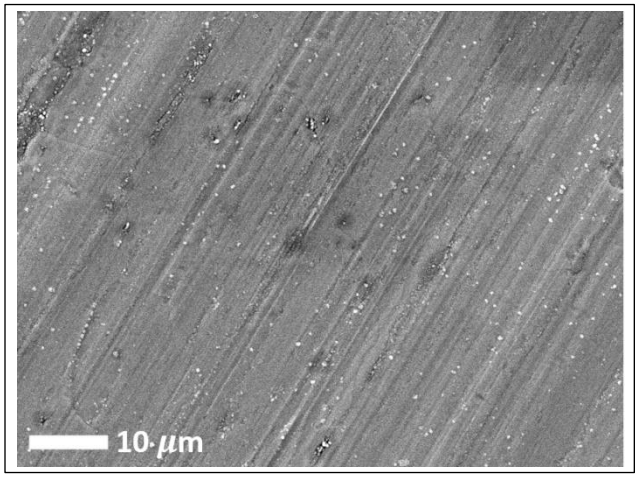

(a) Coated Al immersed in the electrolyte solution with pH=2. Magnification ×1500

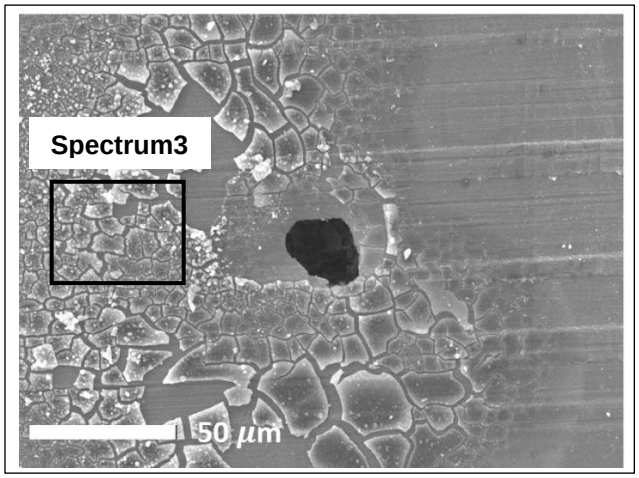

(b) Coated Al immersed in the electrolyte solution with pH=3. Magnification ×500 .

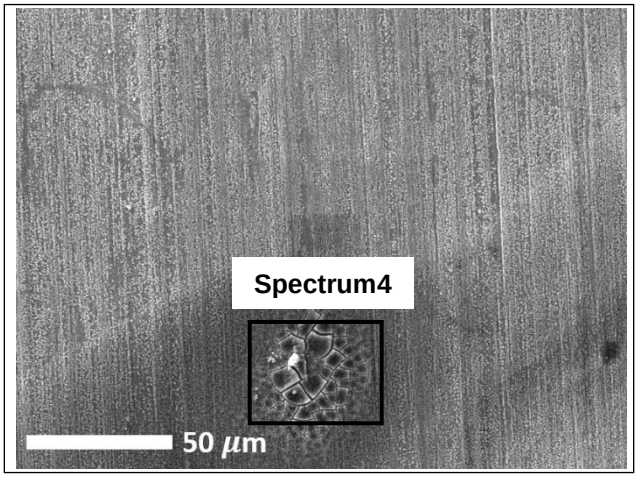

(c) Coated Al immersed in the electrolyte solution with pH=4. Magnification ×500

Figure 4: SEM images of the surface of coated aluminum after LSV measurements, in electrolyte solutions with pH=2, 3 and 4, all solutions containing 3 ppm NaF, solution temperature=80 ℃, start and end potentials for LSV are 50 mV below OCP and 1300 mV vs Ag/AgCl respectively, scan rate=1mVs^{-1}. Spectrum 3 and 4 show places where EDX elemental analysis was performed.

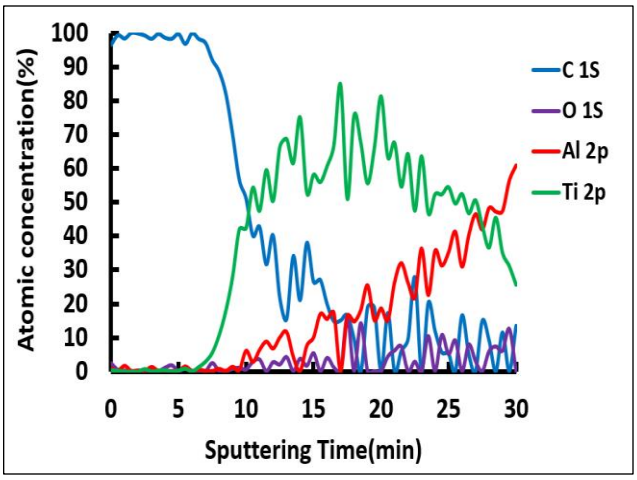

(a) Coated Al before exposure to the electrolyte solutions

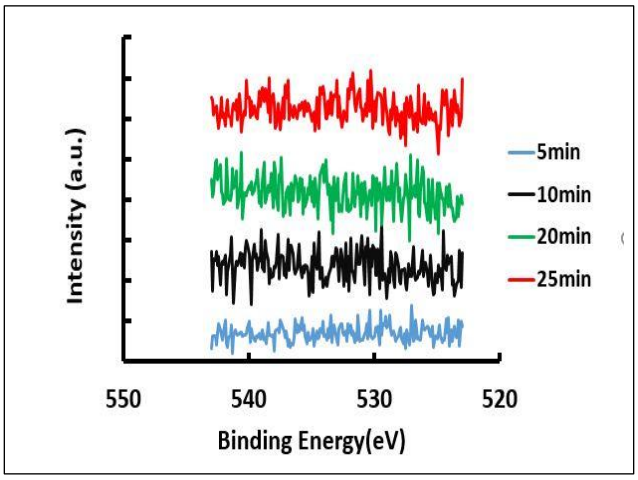

(b) High resolution spectra for O1s for coated Al at different sputtering time before exposure to the electrolyte solutions

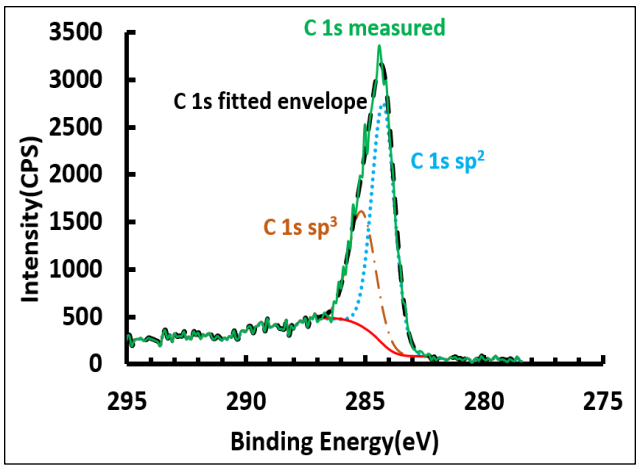

(c) High resolution spectra along with sp^2 and sp^3 peak decomposition for C1s (after 3 minutes sputtering) for coated Al before exposure to the electrolyte solutions

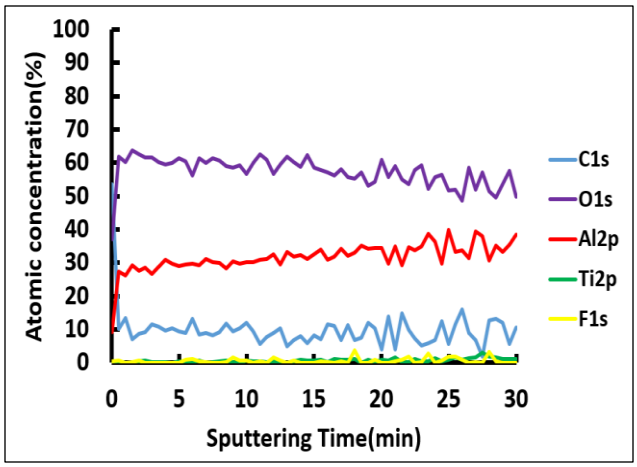

(d) Coated Al immersed in the electrolyte solution with pH=2

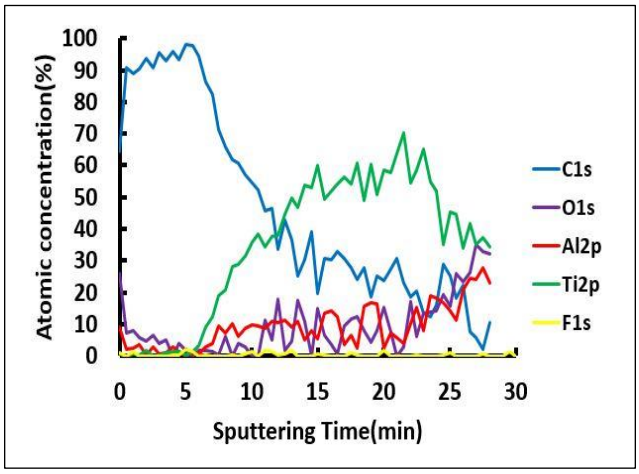

(e) Coated Al immersed in the electrolyte solution with pH=3

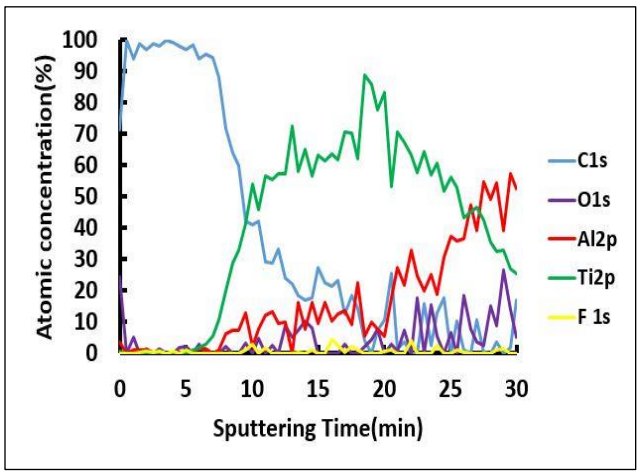

(f) Coated Al immersed in the electrolyte solution with pH=4

Figure 5: XPS depth profiles and elemental analysis for coated Al before and after 24 hours OCP measurements in diluted sulfuric acid solutions with pH=2, 3 and 4 (all solutions contain 3 ppm NaF), solution temperature=80℃.

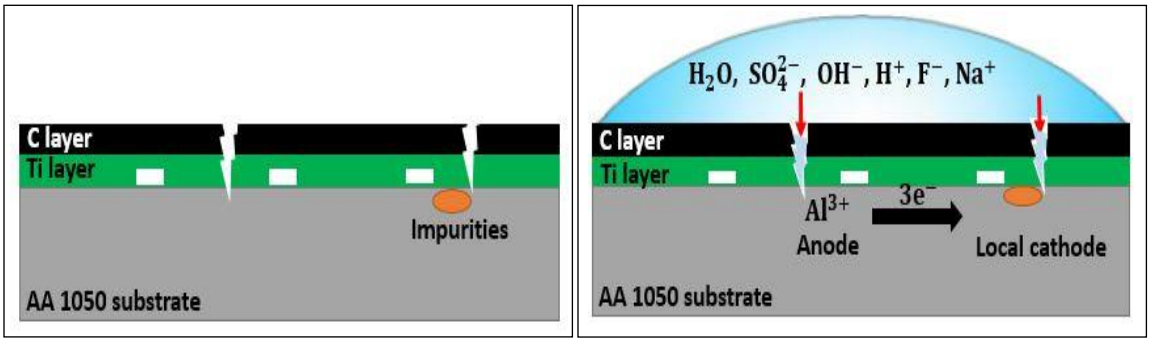

(a) Schematic overview of freshly coated Al (not exposed to the electrolyte). white horizontal rectangles represent the poor adhesion of the coating layer to the substrate. white vertical shapes show the defects in the coating layer

(b) Schematic representation of coated Al immersed in the electrolyte solution along with redox reactions that happen. Red arrows show the direction of the electrolyte which passes through defects in the coating layer and reaches anode and local cathode

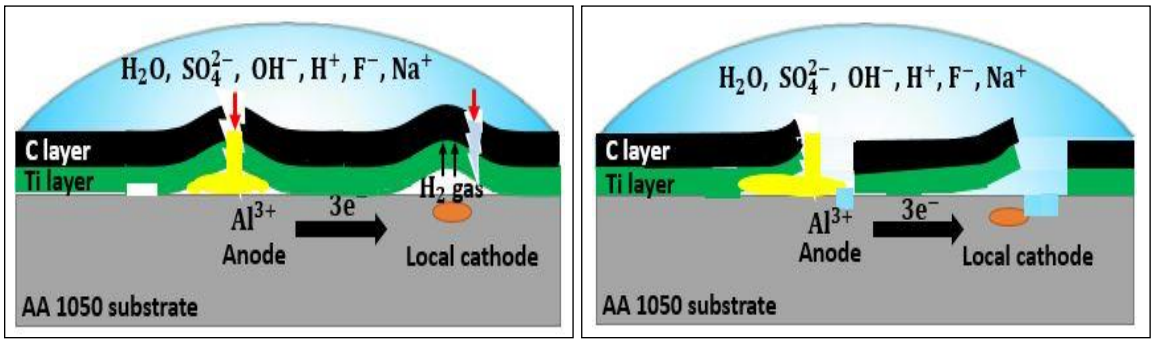

(c) Schematic representation of coated Al after the blistering of the coating layer due to the hydrogen gas evolution and the precipitation of the aluminum oxide and hydroxide shown in yellow color

(d) Schematic representation of coated Al after the failure of the coating layer that the electrolyte solution reaches the underlying substrate and corrodes it

Figure 6: Schematic representation of coated Al, a) before exposure to the electrolyte solution, b) after (initially) immersion in the electrolyte solution containing 3 ppm NaF, c) the blistering of the coating layer by increasing the immersion time, d) complete failure of the coating layer.

Tables and captions:

samples	C	Al	O	Ti	S	F
Coated Al before exposure to the electrolyte (At%)	71	<1	<1	28	0	0
Coated Al after OCP in the electrolyte with pH=2 (At%)	26	45	29	0	0	0
Coated Al after OCP in the electrolyte with pH=3 (spectrum 1) (At%)	5	90	5	0	0	0
Coated Al after OCP in the electrolyte with in pH=3 (spectrum 2) (At%)	56	6	23	13	2	0
Coated Al after OCP in the electrolyte with pH=4 (At%)	70	2	3	25	0	0

Table 1: Quantification for the EDX spectra at 5 kV for coated aluminum before and after 24 hours OCP measurements in the electrolyte solutions with pH=2, 3 and 4 (all solutions containing 3 ppm NaF). Spectrum 1 and 2 are shown in figure 3d.

Samples	C	Al	O	Ti	S	F
Coated Al after LSV in the electrolyte with pH=3 (spectrum 3) (At%)	21	13	53	9	4	0
Coated Al after LSV in the electrolyte with pH=4 (spectrum 4) (At%)	23	14	52	7	3	1

Table 2: Quantification for the EDX spectra at 5 kV for coated aluminum after LSV measurements in electrolyte solutions with pH=3 and 4 (both solutions containing 3 ppm NaF), Spectrum 3 and 4 correspond to coated samples after LSV measurements in electrolyte solutions with pH=3 and 4, respectively. Spectrum 3 and 4 are shown in figure 4.

Peak	BE (eV)	FWHM (eV)	Peak area (%)
C 1s sp^2	284.2	1.1	64
C 1s sp^3	285.1	1.3	36

Table 3: The binding energy (BE), the full width at half maximum (FWHM) and the peak area for sp^2 and sp^3 peaks resulted from C 1s peak decomposition (after 3 minutes sputtering) for coated Al before exposure to the electrolyte solution.

References

[1] A.-C. Dupuis, Proton exchange membranes for fuel cells operated at medium temperatures: Materials and experimental techniques, Progress in Materials Science, 56 (2011) 289-327. https://doi.org/210.1016/j.pmatsci.2010.1011.1001.

[2] Y. Hung, K. El-Khatib, H. Tawfik, Testing and evaluation of aluminum coated bipolar plates of PEM fuel cells operating at 70 C, Journal of Power Sources, 163 (2006) 509-513. https://doi.org/510.1016/j.jpowsour.2006.1009.1013 .

[3] S. Karimi, N. Fraser, B. Roberts, F.R. Foulkes, A review of metallic bipolar plates for proton exchange membrane fuel cells: materials and fabrication methods, Advances in Materials Science and Engineering, 2012 (2012) https://doi.org/10.1155/2012/828070 .

[4] A. Hermann, T. Chaudhuri, P. Spagnol, Bipolar plates for PEM fuel cells: A review, International journal of hydrogen Energy, 30 (2005) 1297-1302. https://doi.org/1210.1016/j.ijhydene.2005.1204.1016 .

[5] P. Mandal, U. kumar Chanda, S. Roy, A review of corrosion resistance method on stainless steel bipolar plate, Materials Today: Proceedings, 5 (2018) 17852-17856. https://doi.org/17810.11016/j.matpr.12018.17806.17111 .

[6] X. Li, I. Sabir, Review of bipolar plates in PEM fuel cells: Flow-field designs, International journal of hydrogen energy, 30 (2005) 359-371. https://doi.org/310.1016/j.ijhydene.2004.1009.1019 .

[7] Y. Yu, H. Li, H. Wang, X.-Z. Yuan, G. Wang, M. Pan, A review on performance degradation of proton exchange membrane fuel cells during startup and shutdown processes: Causes, consequences, and mitigation strategies, Journal of Power Sources, 205 (2012) 10-23. https://doi.org/10.1016/j.jpowsour.2012.1001.1059 .

[8] N.F. Asri, T. Husaini, A.B. Sulong, E.H. Majlan, W.R.W. Daud, Coating of stainless steel and titanium bipolar plates for anticorrosion in PEMFC: A review, International Journal of Hydrogen Energy, 42 (2017) 9135-9148. https://doi.org/9110.1016/j.ijhydene.2016.9106.9241 .

[9] R.A. Antunes, M.C.L. Oliveira, G. Ett, V. Ett, Corrosion of metal bipolar plates for PEM fuel cells: A review, International journal of hydrogen energy, 35 (2010) 3632-3647. https://doi.org/3610.1016/j.ijhydene.2010.3601.3059 .

[10] Y.-C. Park, S.-H. Lee, S.-K. Kim, S. Lim, D.-H. Jung, D.-Y. Lee, S.-Y. Choi, D.-H. Peck, Performance and long-term stability of Ti metal and stainless steels as a metal bipolar plate for a direct methanol fuel cell, International journal of hydrogen energy, 35 (2010) 4320-4328. https://doi.org/4310.1016/j.ijhydene.2010.4302.4010 .

[11] H. Tawfik, Y. Hung, D. Mahajan, Metal bipolar plates for PEM fuel cell—a review, Journal of power sources, 163 (2007) 755-767. https://doi.org/710.1016/j.jpowsour.2006.1009.1088 .

[12] X. Yan, M. Hou, H. Zhang, F. Jing, P. Ming, B. Yi, Performance of PEMFC stack using expanded graphite bipolar plates, Journal of power sources, 160 (2006) 252-257. https://doi.org/210.1016/j.jpowsour.2006.1001.1022 .

[13] A.M. Oladoye, J.G. Carton, A.G. Olabi, Evaluation of CoBlast™ coated titanium alloy as Proton Exchange Membrane fuel cells bipolar plates, J Mater, 2014 (2014) 914817. https://doi.org/914810.911155/912014/914817 .

[14] K. Lin, X. Li, H. Dong, S. Du, Y. Lu, X. Ji, D. Gu, Surface modification of 316 stainless steel with platinum for the application of bipolar plates in high performance proton exchange membrane fuel cells, International journal of hydrogen energy, 42 (2017) 2338-2348. https://doi.org/2310.1016/j.ijhydene.2016.2309.2220 .

[15] P. Yi, D. Zhang, D. Qiu, L. Peng, X. Lai, Carbon-based coatings for metallic bipolar plates used in proton exchange membrane fuel cells, International Journal of Hydrogen Energy, 44 (2019) 6813-6843. https://doi.org/6810.1016/j.ijhydene.2019.6801.6176 .

[16] J.R. Mawdsley, J.D. Carter, X. Wang, S. Niyogi, C.Q. Fan, R. Koc, G. Osterhout, Composite-coated aluminum bipolar plates for PEM fuel cells, Journal of Power Sources, 231 (2013) 106-112. https://doi.org/110.1016/j.jpowsour.2012.1012.1074 .

[17] B. Shabani, M. Hafttananian, S. Khamani, A. Ramiar, A. Ranjbar, Poisoning of proton exchange membrane fuel cells by contaminants and impurities: Review of mechanisms, effects, and mitigation strategies, Journal of Power Sources, 427 (2019) 21-48. https://doi.org/10.1016/j.jpowsour.2019.1003.1097 .
[18] S.A.A. El-Enin, O.E. Abdel-Salam, H. El-Abd, A.M. Amin, New electroplated aluminum bipolar plate for PEM fuel cell, Journal of Power Sources, 177 (2008) 131-136. https://doi.org/110.1016/j.jpowsour.2007.1011.1042 .
[19] E.M. Gabreab, G. Hinds, S. Fearn, D. Hodgson, J. Millichamp, P.R. Shearing, D.J. Brett, An electrochemical treatment to improve corrosion and contact resistance of stainless steel bipolar plates used in polymer electrolyte fuel cells, Journal of Power Sources, 245 (2014) 1014-1026. https://doi.org/1010.1016/j.jpowsour.2013.1007.1041 .
[20] S. Joseph, J. McClure, P. Sebastian, J. Moreira, E. Valenzuela, Polyaniline and polypyrrole coatings on aluminum for PEM fuel cell bipolar plates, Journal of Power Sources, 177 (2008) 161-166. https://doi.org/110.1016/j.jpowsour.2007.1009.1113 .
[21] C.-H. Lin, S.-Y. Tsai, An investigation of coated aluminium bipolar plates for PEMFC, Applied energy, 100 (2012) 87-92. https://doi:10.1016/j.apenergy.2012.1006.1045 .
[22] H. Sun, K. Cooke, G. Eitzinger, P. Hamilton, B. Pollet, Development of PVD coatings for PEMFC metallic bipolar plates, Thin Solid Films, 528 (2013) 199-204. https://doi.org/110.1016/j.tsf.2012.1010.1094 .
[23] Z. Wang, H. Hu, C. Liu, Y. Zheng, The effect of fluoride ions on the corrosion behavior of pure titanium in 0.05 M sulfuric acid, Electrochimica acta, 135 (2014) 526-535. https://doi.org/510.1016/j.electacta.2014.1005.1055 .
[24] W.-Y. Ho, H.-J. Pan, C.-L. Chang, D.-Y. Wang, J.J. Hwang, Corrosion and electrical properties of multi-layered coatings on stainless steel for PEMFC bipolar plate applications, Surface and Coatings Technology, 202 (2007) 1297-1301. https://doi.org/1210.1016/j.surfcoat.2007.1207.1056 .
[25] K. Feng, Y. Shen, H. Sun, D. Liu, Q. An, X. Cai, P.K. Chu, Conductive amorphous carbon-coated 316L stainless steel as bipolar plates in polymer electrolyte membrane fuel cells, International journal of hydrogen energy, 34 (2009) 6771-6777. https://doi.org/6710.1016/j.ijhydene.2009.6706.6030 .
[26] A. Kumar, M. Ricketts, S. Hirano, Ex situ evaluation of nanometer range gold coating on stainless steel substrate for automotive polymer electrolyte membrane fuel cell bipolar plate, Journal of Power Sources, 195 (2010) 1401-1407. https://doi.org/1410.1016/j.jpowsour.2009.1409.1022 .
[27] S.-J. Lee, C.-H. Huang, Y.-P. Chen, C.-T. Hsu, PVD Coated Bipolar Plates for PEM Fuel Cells, Journal of Fuel Cell Science and Technology, 2 (2005) 290-294. https://doi.org/210.1115/1111.2041671 .
[28] P. Yi, X. Li, L. Yao, F. Fan, L. Peng, X. Lai, A lifetime prediction model for coated metallic bipolar plates in proton exchange membrane fuel cells, Energy Conversion and Management, 183 (2019) 65-72. https://doi.org/10.1016/j.enconman.2018.1012.1092 .
[29] P. Zhang, C. Hao, Y. Han, F. Du, H. Wang, X. Wang, J. Sun, Electrochemical behavior and surface conductivity of NbC modified Ti bipolar plate for proton exchange membrane fuel cell, Surface and Coatings Technology, 397 (2020) 126064. https://doi.org/126010.121016/j.surfcoat.122020.126064 .
[30] J.G. Reynolds, J.D. Belsher, A review of sodium fluoride solubility in water, Journal of Chemical & Engineering Data, 62 (2017) 1743-1748. https://doi.org/1710.1021/acs.jced.1747b00089 .
[31] T. Xue, W. Cooper, R. Pascual, S. Saimoto, Effect of fluoride ions on the corrosion of aluminium in sulphuric acid and zinc electrolyte, Journal of applied electrochemistry, 21 (1991) 238-246. https://doi.org/210.1007/BF01052577 .
[32] C. Vargel, Corrosion of aluminium, Elsevier, Amsterdam; Boston, 2004. http://www.books24x7.com/marc.asp?bookid=37295.
[33] J. Cerezo, I. Vandendael, R. Posner, K. Lill, J. De Wit, J. Mol, H. Terryn, Initiation and growth of modified Zr-based conversion coatings on multi-metal surfaces, Surface and Coatings Technology, 236 (2013) 284-289. https://doi.org/210.1016/j.surfcoat.2013.1009.1059 .
[34] Y. Murata, S. Ohtani, Measurement of the growth of oxide layers on metals by low-energy electron spectroscopy: aluminum, Journal of Vacuum Science and Technology, 9 (1972) 789-791.

https://doi.org/710.1116/1111.1317783 .
[35] N. Cabrera, N.F. Mott, Theory of the oxidation of metals, Reports on progress in physics, 12 (1949) 163-184. https://doi.org/110.1088/0034-4885/1012/1081/1308 .
[36] Thermo scientific XPS, https://xpssimplified.com/elements/oxygen. php. Last access: 21/12/2020.
[37] D.R. Baer, M.H. Engelhard, A.S. Lea, P. Nachimuthu, T.C. Droubay, J. Kim, B. Lee, C. Mathews, R. Opila, L.V. Saraf, Comparison of the sputter rates of oxide films relative to the sputter rate of SiO 2, Journal of Vacuum Science & Technology A: Vacuum, Surfaces, and Films, 28 (2010) 1060-1072. https://doi.org/1010.1116/1061.3456123 .
[38] J. Diaz, G. Paolicelli, S. Ferrer, F. Comin, Separation of the sp 3 and sp 2 components in the C1s photoemission spectra of amorphous carbon films, Physical Review B, 54 (1996) 8064, https://doi.org/8010.1103/PhysRevB.8054.8064.
[39] T. Leung, W. Man, P. Lim, W. Chan, F. Gaspari, S. Zukotynski, Determination of the sp3/sp2 ratio of aC: H by XPS and XAES, Journal of non-crystalline solids, 254 (1999) 156-160. https://doi.org/110.1016/S0022-3093(1099)00388-00389.
[40] K. Feng, X. Cai, H. Sun, Z. Li, P.K. Chu, Carbon coated stainless steel bipolar plates in polymer electrolyte membrane fuel cells, Diamond and Related Materials, 19 (2010) 1354-1361. https://doi.org/1310.1016/j.diamond.2010.1307.1003.
[41] M. Pourbaix, Atlas of electrochemical equilibria in aqueous solution, NACE, 307 (1974).
[42] N.S. Greg Monaghan, Ben Estill, Victoria Winston, Paint and coatings industry, Metal Adhesion and Corrosion Resistance of Coatings, 2018, Access date "29/04/2021", https://www.pcimag.com/articles/104787-metal-adhesion-and-corrosion-resistance-of-coatings .
[43] T. Hurlen, K. Johansen, Effect of fluoride ions on corrosion and passive behavior of aluminium, ACTA CHEMICA SCANDINAVICA SERIES A-PHYSICAL AND INORGANIC CHEMISTRY, 39 (1985) 545-551. https://doi:510.3891/acta.chem.scand.3839a–0545 .
[44] T. Våland, G. Nilsson, The influence of F− ions on the electrochemical reactions on oxide-covered A1, Corrosion science, 17 (1977) 449-459. https://doi.org/410.1016/0010–1938X(1077)90001–90004 .